CrossMark

A facile method to enhance electrochemical performance of high-nickel cathode material Li(Ni$_{0.8}$Co$_{0.1}$Mn$_{0.1}$)O$_2$ via Ti doping

Jiawei Li[1] · Ying Li[1] · Yongnan Guo[2,4] · Jiale Lv[2] · Wentao Yi[3] · Peihua Ma[1]

Abstract

The cycle stability of Li(Ni$_{0.8}$Co$_{0.1}$Mn$_{0.1}$)O$_2$ is enhanced obviously by titanium doping via a facile solid-state method. The property of crystal structure is evaluated by XRD, which illustrates the samples possessed a layered α-NaFeO$_2$ structure with R-3m space group. According to the charge/discharge studies, the capacity retention of pristine sample is around 51% after 125 cycles at 5 C, and the sample with Ti dopant displays a good cyclic stability, after 125 cycles, the capacity retention increases to 75% under 5 C, suggesting it could be possibly applied in fast charge Lithium-ion battery area. The superb electrochemical performance might be attributed to the Ti^{4+} occupy the layer structure to broaden the Lithium-ion channel, which is benefit to lithium intercalation and deintercalation during cycling.

1 Introduction

The demand of Lithium-ion batteries (LIBs) has gradually became larger in electric vehicles (EVs), hybrid electric vehicles (HEVs), and energy storage systems [1–4]. That will bring an enormous challenge to the electrochemical performance of LIBs, especially when some European countries start to make policy to ban oil-fueled automobile in 2040s or earlier. High-nickel cathode material has the potential to develop into the next generation of power battery, because of the high capacity, tap density and working voltage [5, 6]. Among all high-nickel cathode materials, Li(Ni$_{0.8}$Co$_{0.1}$Mn$_{0.1}$)O$_2$ has better electrochemical properties, its reversible capacity could reach 200 mAh/g, under the potential range of 2.5–4.3 V [7–10], while other Ni-rich cathode materials, such as Li(Ni$_{0.6}$Co$_{0.2}$Mn$_{0.2}$)O$_2$ and

Li(Ni$_{0.5}$Co$_{0.2}$Mn$_{0.3}$)O$_2$ only have 180 and 170 mAh/g discharge capacity in the same range of voltage respectively [11–13]. Although Li(Ni$_{0.8}$Co$_{0.1}$Mn$_{0.1}$)O$_2$ possesses high reversible capacity, it still has several problems limit its rapid development, for instants, its capacity retention and safety performance. One reason to cause those problems is that Ni/Li ion disorder, previous studies have reported that unstable Ni^{4+} ions in cathode materials will transform into Ni^{2+} ions in delithiated process, Ni^{2+} and Li$^+$ possess similar particle size, therefore, Ni^{2+} will irreversibly deintercalate from transition metal layers and occupy Li$^+$ positions, to form inactive NiO-type rock-salt phases [14, 15]. Other studies also reported that, excessed LiOH or LiCO$_3$ in cathode materials would easily absorb moisture when expose in air, to generate impurity phases on the surface cathode particle [16, 17]. With the aim of solving these problems, numerous efforts have been taken to pursue a proper solution. One of the most common and effective methods to enhance the electrochemical properties and thermal stability is surface coating, such as MgF$_2$, AlPO$_4$, Al$_2$O$_3$, Co$_3$O$_4$, LiSiO$_3$, LiF, LiVO$_4$ [18–24]. The coating of the surface can prevent electrolyte attack, and reduce decomposition of active materials, therefore, the capacity retention can raise up obviously. For instance, the capacity retention of sample with and without LiVO$_4$ coating, are 87.3 and 58.8% respectively, after 100 cycles under 1 C rate. Recently, there is another effective method has frequently been reported, which is preparing core–shell structure cathode materials. Lu et al. [25] coated Li(Ni$_{1/3}$Co$_{1/3}$Mn$_{1/3}$)O$_2$ onto Li(Ni$_{0.8}$Co$_{0.1}$Mn$_{0.1}$)O$_2$,

✉ Ying Li
liying@smm.neu.edu.cn

1 School of Metallurgy, Northeastern University, No. 3-11, Wenhua Road, Heping District, Shenyang 110819, People's Republic of China

2 Jiangsu Lithitech Co. Ltd, Changzhou 213300, People's Republic of China

3 College of Chemistry, Chemical Engineering and Materials Science, Zaozhuang University, Zaozhuang 277160, People's Republic of China

4 College of Materials Science and Engineering, Hunan University, Changsha 410082, People's Republic of China

increase 5.47% of capacity retention in 2 C after 100 times. Yoo et al. [26] successfully prepare $xLi(Ni_{0.8}Co_{0.15}Al_{0.05})O_2 \cdot (1-x)Li(Ni_{0.6}Co_{0.1}Mn_{0.3})O_2$, the capacity retention increased from 89.94 to 99.27% after 50 cycles. The benefit of core–shell structure, when compares to inactive coating, is that core–shell structure coated by an active shell, not only prevent electrolyte contact, also provide lithium ion in charge and discharge reaction. However, the process of synthesis is relatively complex, leading to the increasing complexity of production technology in manufactory. In this report, a facile method will be used to dope Ti^{4+} into the layer structure of $Li(Ni_{0.8}Co_{0.1}Mn_{0.1})O_2$, and enormously enhance the capacity retention, especially in high current charging and discharging processes.

2 Experimental

The $Ni_{0.8}Co_{0.1}Mn_{0.1}(OH)_2$ precursor was synthesized via co-precipitation method, three appropriate amount of solutions were pumped into a 20 L continuously stirring tank reactor with the same speed, respectively, (1) a 2 M mixture solution of $NiSO_4 \cdot 6H_2O$, $CoSO_4 \cdot 6H_2O$, and $MnSO_4 \cdot H_2O$ with a cation molar ratio of 8:1:1; (2) 4 M NaOH solution and (3) 2 M NH_4OH solution as precipitation chelating agent. The pH of the reaction was controlled in 11.5 via an online pH meter and kept the temperature of 53 °C under nitrogen atmosphere. To obtain the $Ni_{0.8}Co_{0.1}Mn_{0.1}(OH)_2$ precursor, the reaction continually performed 16 h, and followed by aging 4 h. The slurry was washed, then filtered in a suction filter equipment and dried at 100 °C in vacuum drying oven.

$Li(Ni_{0.8}Co_{0.1}Mn_{0.1})O_2$ with Ti^{4+} dopant was synthesized via solid-state method. The process of the method illustrates in Fig. 1. Firstly, mixed stoichiometric of $Ni_{0.8}Co_{0.1}Mn_{0.1}(OH)_2$ precursor and 5 wt% excess of LiOH together in a ball mill, at the same time, added a certain amount of nano-TiO_2 into the mixture (3 wt%), and began to grind for a while. Secondly, transferred the mixture into a saggar and sintered in an atmosphere muffle furnace, pre-heated to 480 °C for 5 h, and then heated to 750 °C for 15 h.

The crystal structure of synthesized samples was detected by X-ray powder diffraction (XRD, Shimadzu XRD-6100), with Cu-Ka radiation in the 2θ range from 10° to 80° at the step of 1°/min. The particle morphology of the samples were observed by a scanning electron microscope (SEM, JSM-7800F, JEOL), the element contents on the surface of the particles were identified by SEM as well.

The electrochemical properties were tested using CR2032 coin-type cells. The preparation processes of the electrode are as followed: Pour a certain amount of N-methyl-2-pyrrolidone (NMP) into a container as the base solution of the slurry, then 80% active material, 10% super P and 10% polyvinylidene fluoride (PVDF) were added into the container and stirred overnight, followed by coating on an aluminum foil. After being dried in a vacuum oven at 120 °C for 10 h, the electrode was cut in a circle shape and pressed under 1 MPa pressure. The coin-type cells were assembled in a glove box with Ar atmosphere protection, the electrolyte using 1 M LiPF6 in ethylene carbonate and diethyl carbonate (EC/DEC = 1:1) solution, the anode choose the pure lithium electrode. Afterwards, cells were measured by charge and discharge tester (Neware, CT-3008). The cyclic voltammetry (CV) curves were tested by electrochemical workstation (EPSILON BAS), between 2.8 and 4.4 V at a scan rate of 0.2 mV/s, and electrochemical impedance spectroscopy (EIS) were measured by the same electrochemical workstation with a voltage of 5 mV amplitude over a frequency range from 100 KHz to 0.1 Hz.

3 Results and discussion

Figure 2 shows the XRD patterns of $Li(Ni_{0.8}Co_{0.1}Mn_{0.1})O_2$ sample (pristine NCM811) and $Li(Ni_{0.8}Co_{0.1}Mn_{0.1})O_2$ with titanium dopant sample (T-NCM811), the composite of both XRD patterns illustrate a clear layered structure, in possession of a hexagonal a-$NaFeO_2$ structure with an R-3m space group. No different diffraction peak emerges in the T-NCM811 XRD pattern, which indicates no impurity phases in T-NCM811 sample, probably due to titanium
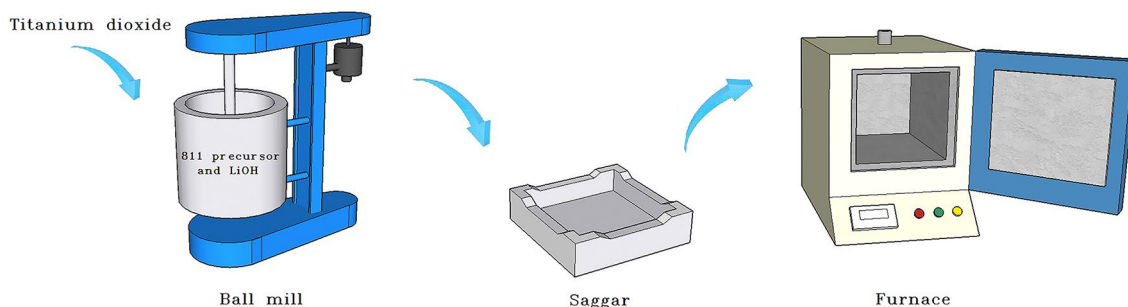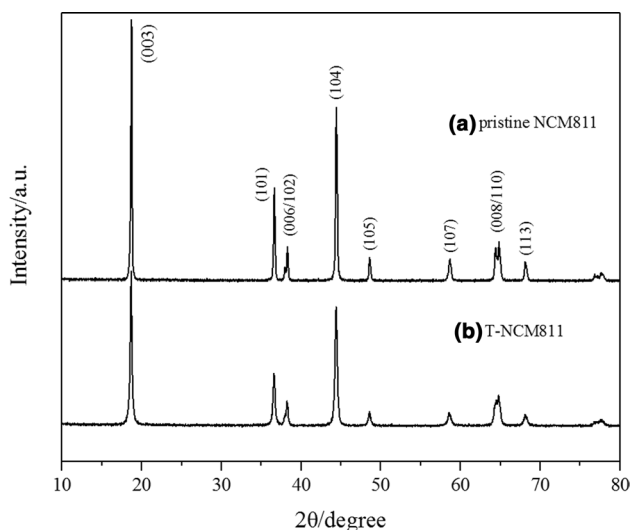

Fig. 1 Process of solid-state synthesis method

Fig. 2 XRD patterns of (*a*) pristine NCM811 sample and (*b*) T-NCM811 sample

ions sintered into the crystal texture of the NCM811 well. The clearly observed splitting peak 006/102 and 008/110 illustrate both of the samples own a highly ordered layer structure [27, 28]. The lattice constants of a and c of T-NCM811 are respectively 2.8769 and 14.2305 Å, which are larger than the constants of pristine NCM811 sample, 2.8749 and 14.2039 Å. Because the radii of Ni^{3+} (0.56 Å), Co^{3+} (0.545 Å), Mn^{4+} (0.53 Å) and Ti^{4+} (0.605 Å) are different [29, 30], the lattice spacing has been enlarged when the titanium ions occupy the transitional metal positions after calcination.

Figure 3 presents the SEM images of the pristine sample (Fig. 3a) and the sample with titanium dopant (Fig. 3b). According to the left part of the two images, both of the samples possess a spheroidal morphology with the size between 5 and 15 μm. On the right-hand side of picture (a) and (b), uniform polyhedral primary sedimentation particles can be clearly observed, size from 100 to 500 nm. Comparing with the two pictures, no noticeable difference can be seen in (a) and (b), which suggesting titanium has possibly well doped into the NCM811 crystal structure and titanium dopant cannot damage the surface morphology of the NCM811 particles.
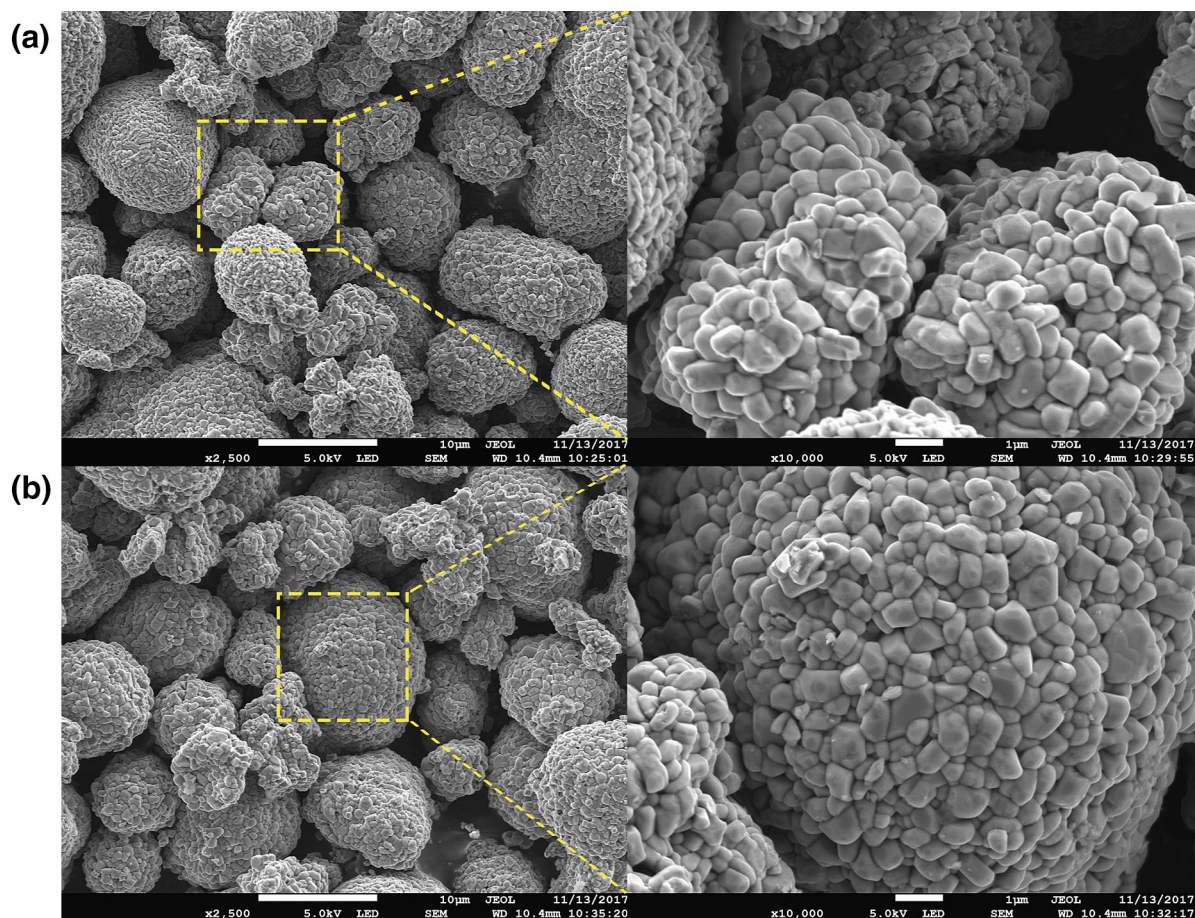

Fig. 3 SEM images of **a** NCM811 sample and **b** T-NCM811 sample

To further investigate the result of doping, EDS spectra was performed to detect the element contents on the surface of the particles. Figure 4 shows the EDS spectra of T-NCM811 sample, titanium peaks were detected, which indicate titanium has doped into particle. Furthermore, the wt% of titanium shows in Table 1 is 1.82%, approach to the theoretical content of 1.798%, indicating titanium has been wholly doping into target.
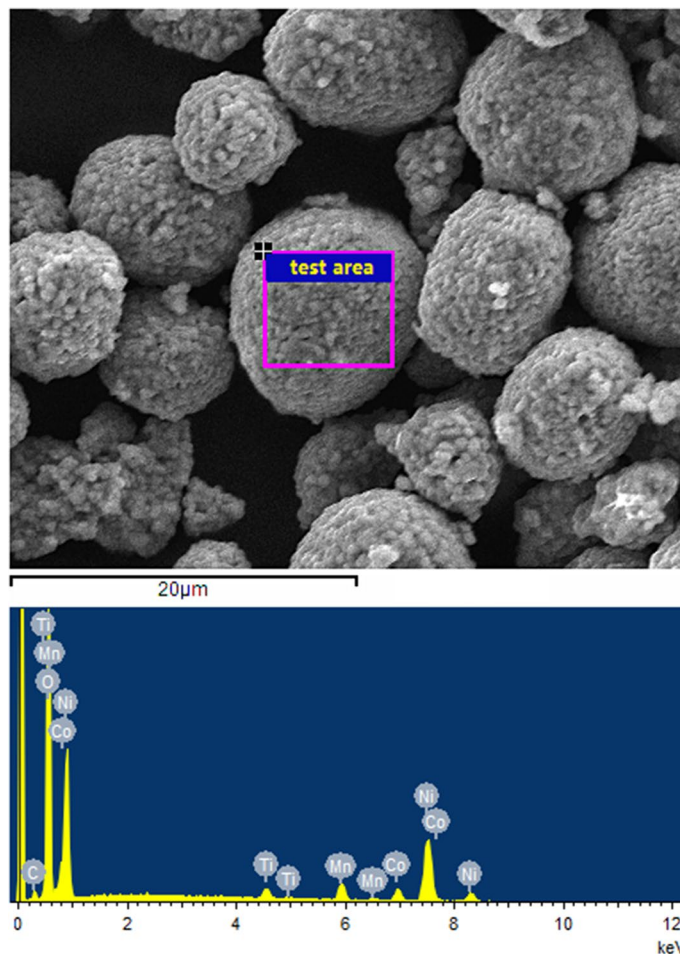
Figure 5a and b illustrate the CV curves of the pristine NCM811 and T-NCM811 samples, the potential range tested from 2.8 to 4.4 V (vs Li/Li$^+$) with a scanning rate of 0.1 mV/s. In the initial two cycles, the patterns for both two samples display two pairs of reversible redox peaks. In the first pair of redox peaks, cathodic peaks appear around 3.8–4.1 V, due to the oxidation of Ni^{2+} to Ni^{3+} and Ni^{3+} to Ni^{4+}, anodic peaks emerge at 3.6–3.7 V, corresponds to the reduction reaction of Ni^{4+} to Ni^{3+} and Ni^{3+} to Ni^{2+}. The second pair of redox formed by the oxidizing reaction of Co^{3+} to Co^{4+} and reduction reaction of Co^{4+} to Co^{3+}, at the potential range of 4.2 to 4.3 and 4.1 to 4.2 V, respectively [31, 32]. When compares the first and the second cycle of the CV curves, the cathodic peak potential of the first cycle is larger than that in second cycle, mainly because the irreversible reactions occur in the initial charging, such as the formation of the SEI film. When compares to the curves of pristine NCM811 and T-NCM811, the potential difference between the oxidation and reduction peaks is much larger for the T-NCM811 sample, indicating the electrode polarization has been increased in the initial two cycles when doping titanium ion into the NCM811.

Table 1 EDS parameters of T-NCM811 sample

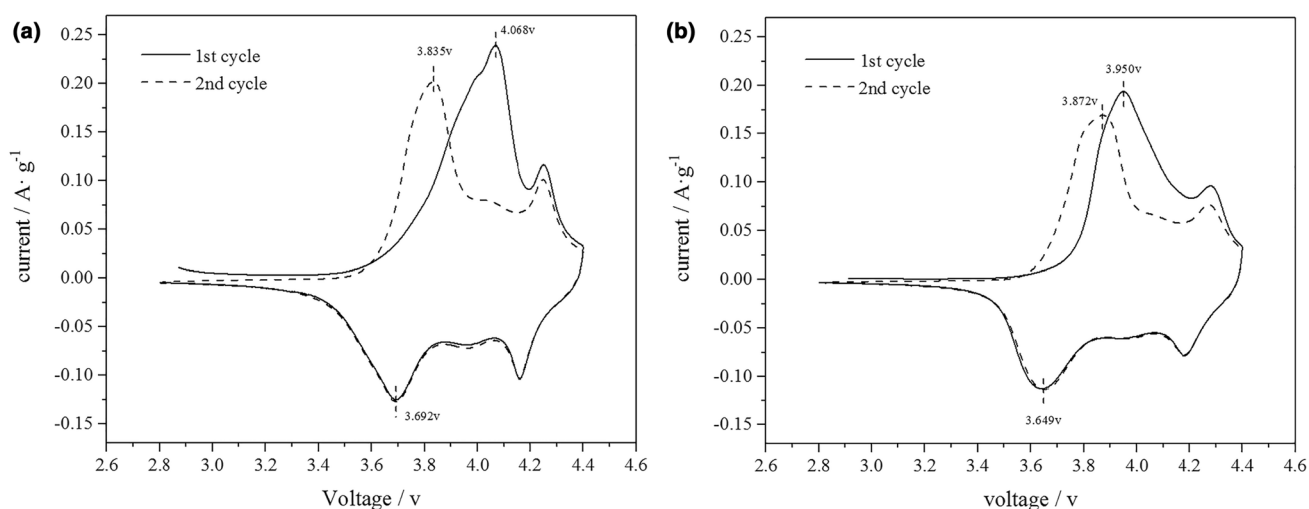| Element	Weight percentage (%)	Atomic percentage (%)
C K	3.03	7.01
O K	37.07	64.32
Ti K	1.82	1.05
Mn K	5.46	2.76
Co K	6.36	3.00
Ni K	46.25	21.87

Fig. 4 EDS image of T-NCM811 sample

Fig. 5 CV curves of pristine **a** NCM811 and **b** T-NCM811 samples

Figure 6 shows the charge and discharge study curves of pristine NCM811 and T-NCM811. Figure 6a shows the initial charge and discharge curves of two samples, the initial charge capacity for pristine NCM811 and T-NCM811 are 242.13 and 235.31 mAh/g, and initial discharge capacity are 199.52 and 190.23 mAh/g, charge–discharge efficiency are 82.40 and 80.84%, respectively. Figure 6b presents the discharge ability in various current density of the two samples, including 0.1, 0.2, 0.5, 1, 2, 3 and 5 C, under the potential range of 2.5 to 4.3 V at room temperature. With the current flow increase, the reversible capacity reduce obviously, due to the increasing polarization. The initial reversible capacity of T-NCM811 is a bit less than that of pristine NCM811 at the same current rate. This can be explained by two reasons: First, when doping titanium ions into the electrode, which are inactive contents for lithium-ion batteries, the ratio of the active material will decrease, leading the capacity lower than pristine material. Second, the polarization increase in the sample with titanium dopant also results in the reduction of the reversible capacity. Figure 6c compares the capacity retention in 5C current flow of pristine NCM811 and T-NCM811 composite electrodes, the initial discharge capacity of pristine NCM811 is 151 mAh/g, which is higher than that of the T-NCM811, 144 mAh/g. However, when the cycle times increase, the capacity of the NCM811 reduce sharply. After 125 times the capacity only remains 78 mAh/g, 51.65% of the initial capacity. T-NCM811 sample retains much more reversible capacity, after 125 cycles the T-NCM811 sample still remains 108 mAh/g, 75.0% of the initial capacity, even after 200 cycles, the reversible capacity only reduce to 97 mAh/g, still possesses 67.36% of the initial capacity.

To further understand the enhancement of the capacity retention of NCM811 with titanium dopant, EIS measurements were carried out for both pristine NCM811 and T-NCM811 after 50 cycles, shown in Fig. 7. Both of the Nyquist curves in Fig. 7 present two semicircles and a Warburg region. The first semicircle in high frequency refers to the surface film resistance R_{sei}, with its capacitance C_{sei}, the second semicircle in medium frequency stands for the resistance and capacitance of charge-transfer, R_{ct} and C_{ct}. The fitted values of R_{sei} are 10.2 and 13.7 Ω, and R_{ct} are 15.5 and 20.3 Ω for pristine NCM811 and T-NCM811, respectively. It can be seen that both of the Rsei and Rct after 50 cycles in T-NCM811 sample are smaller than those in pristine NCM811 sample. Therefore, the titanium dopant in T-NCM811 can enlarge the transfer channel of lithium ion to reduce the resistance increase, which results in outstanding improvement of the capacity retention.

The thermal decomposition behavior of pristine NCM811 and T-NCM811 were investigated by TGA, which presents in Fig. 8. From 0 to 750 °C, the weight loss of both materials are not obvious, this process is mainly attributed to the removal of absorb water and decomposition of impurities. The decomposition of the pristine NCM811 and T-NCM811 start from the temperature of 750 °C. The mass retention of pristine NCM811 sample reduce 5.9%, between 750 and 1150 °C, while T-NCM811 only lose 4.3% of its weight. The data of TGA illustrate the thermal stability of T-NCM811 is superior than pristine NCM811 sample, and indirectly explain that, the T-NCM811 sample possesses better cycling stability than pristine NCM811 sample, especially in high current flow.

4 Conclusion

In sum, NCM811 with titanium dopant performs a better capacity retention, mainly attributed to the following factors: (1) the titanium ions doping into the lattice structure,
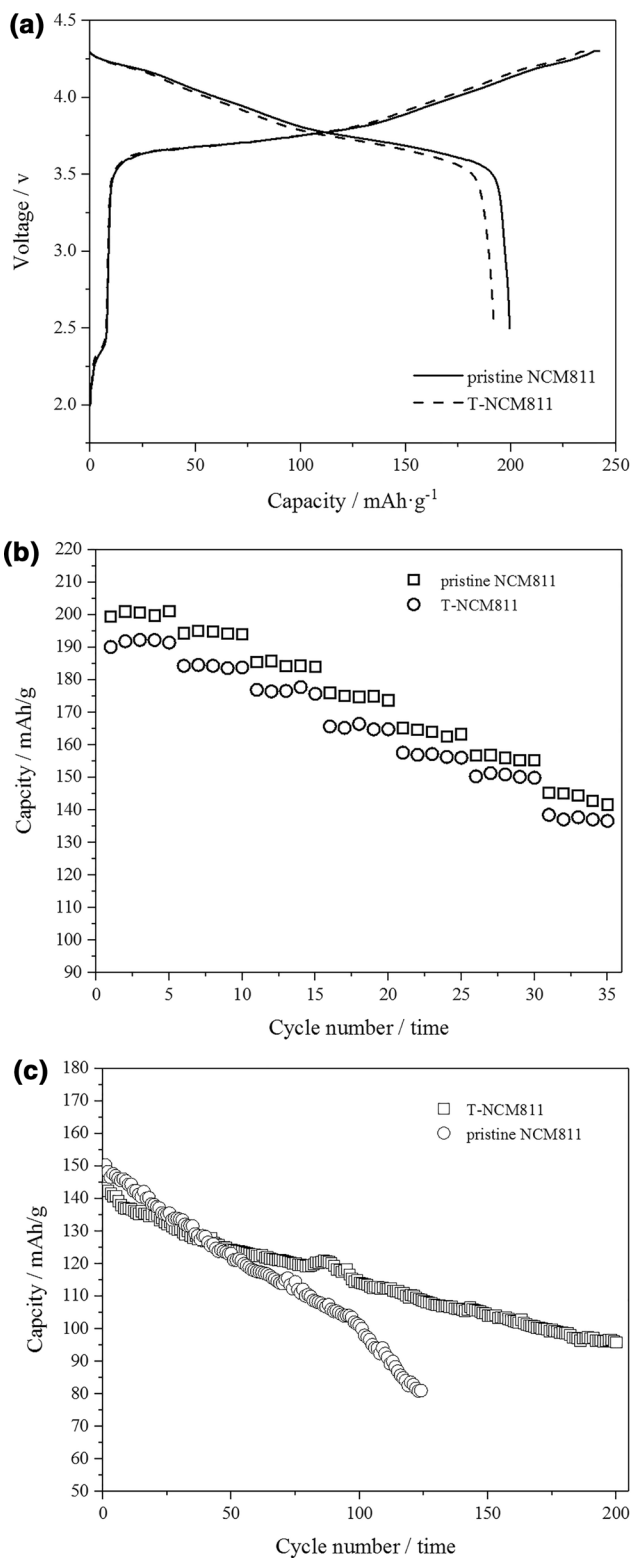
Fig. 6 Charge and discharge study curves of **a** initial charge and discharge curves **b** rate test curves and **c** cycling performance at 5 C
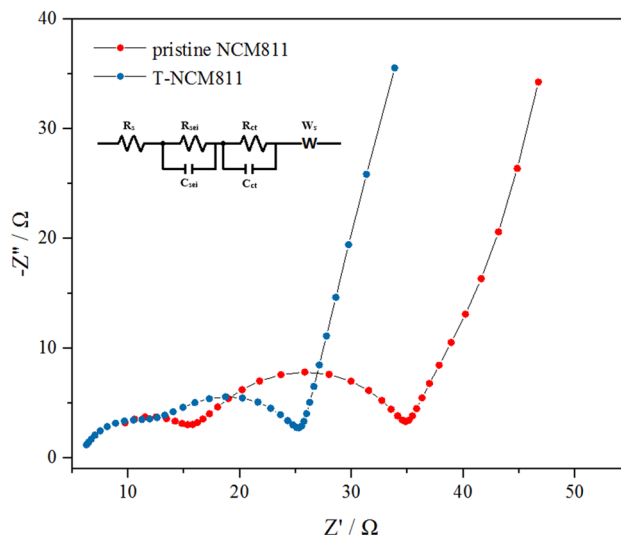

Fig. 7 Nyquist curves of pristine NCM811 and T-NCM811 after 50 cycles
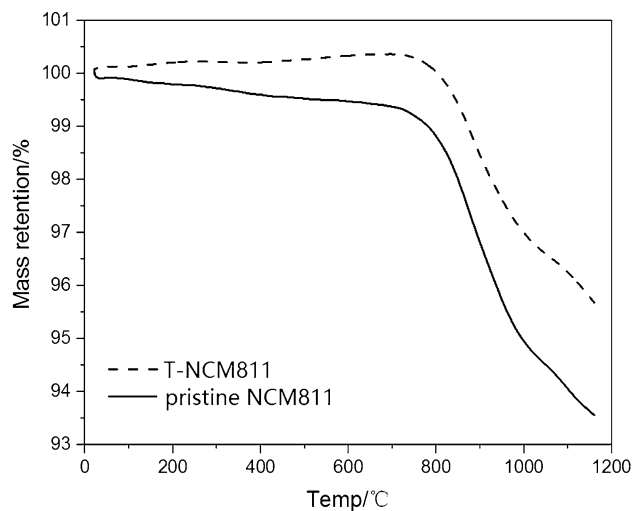

Fig. 8 TGA curves of pristine NCM811 and T-NCM811

can broaden interslab distances and stable the crystal structure, reduce impedance after cycles. This factor is benefit to lithium intercalation and deintercalation (2) titanium ions into the lattice structure can prevent decomposition of cathode materials, especially in high discharge rate. In addition, the better performance of T-NCM811 in a relative high discharge rate suggesting a possible application in fast charge Lithium-ion batteries area. Furthermore, the facile method can reduce the cost of production and can make the improvement of existing production line without new facilities.

References

1. A.S. Aricò, P. Bruce, B. Scrosati, J.-M. Tarascon, W. van Schalkwijk, Nat. Mater. **4**:366 (2005). https://doi.org/10.1038/nmat1368
2. B. Dunn, H. Kamath, J.-M. Tarascon, Science **334**, 928 (2011)
3. N.-S. Choi, Z. Chen, S.A. Freunberger et al., Angew. Chem. Int. Ed. **51**, 9994 (2012). https://doi.org/10.1002/anie.201201429
4. S.-M. Bak, K.-W. Nam, W. Chang et al., Chem. Mater. **25**, 337 (2013). https://doi.org/10.1021/cm303096e
5. S. Hwang, S.M. Kim, S.-M. Bak et al., ACS Appl. Mater. Interfaces **6**, 15140 (2014). https://doi.org/10.1021/am503278f
6. Y.-K. Sun, S.-T. Myung, B.-C. Park, K. Amine, Chem. Mater. **18**, 5159 (2006). https://doi.org/10.1021/cm061746k
7. X. Zheng, X. Li, B. Zhang et al., Ceram. Int. **42**, 644 (2016). https://doi.org/10.1016/j.ceramint.2015.08.159
8. S.S. Jan, S. Nurgul, X. Shi, H. Xia, H. Pang, Electrochim. Acta **149**, 86 (2014). https://doi.org/10.1016/j.electacta.2014.10.093
9. C. Hua, K. Du, C. Tan, Z. Peng, Y. Cao, G. Hu, J. Alloy. Compd. **614**, 264 (2014). https://doi.org/10.1016/j.jallcom.2014.06.049
10. C. Zhang, J. Qi, H. Zhao et al., Mater. Lett. **201**, 1 (2017). https://doi.org/10.1016/j.matlet.2017.04.121
11. Z. Huang, Z. Wang, Q. Jing, H. Guo, X. Li, Z. Yang, Electrochim. Acta **192**, 120 (2016). https://doi.org/10.1016/j.electacta.2016.01.139
12. Y. Huang, F.-M. Jin, F.-J. Chen, L. Chen, J. Power Sources **256**, 1 (2014). https://doi.org/10.1016/j.jpowsour.2014.01.003
13. K. Liu, G.-L. Yang, Y. Dong, T. Shi, L. Chen, J. Power Sources **281**, 370 (2015). https://doi.org/10.1016/j.jpowsour.2014.12.131
14. S.U. Woo, C.S. Yoon, K. Amine, I. Belharouak, Y.K. Sun, J. Electrochem. Soc. **154**, A1005 (2007)
15. S.W. Song, G.V. Zhuang, P.N. Ross, J. Electrochem. Soc. **151**, A1162 (2004)
16. B.J. Neudecker, R.A. Zuhr, B.S. Kwak, J.B. Bates, J.D. Robertson, J. Electrochem. Soc. **145**, 4148 (1998)
17. D.P. Abraham, R.D. Twesten, M. Balasubramanian, I. Petrov, J. McBreen, K. Amine, Electrochem. Commun. **4**, 620 (2002). https://doi.org/10.1016/S1388-2481(02)00388-0
18. P.R. Ilango, T. Subburaj, K. Prasanna, Y.N. Jo, C.W. Lee, Mater. Chem. Phys. **158**, 45 (2015). https://doi.org/10.1016/j.matchemphys.2015.03.033
19. K. Araki, N. Taguchi, H. Sakaebe, K. Tatsumi, Z. Ogumi, J. Power Sources **269**, 236 (2014). https://doi.org/10.1016/j.jpowsour.2014.06.101
20. Y. Huang, Y. Huang, X. Hu, Electrochim. Acta **231**, 294 (2017). https://doi.org/10.1016/j.electacta.2017.02.067
21. H. Meng, P. Zhou, Z. Zhang, Z. Tao, J. Chen, Ceram. Int. **43**, 3885 (2017). https://doi.org/10.1016/j.ceramint.2016.12.054
22. Z. Qiu, Y. Zhang, P. Dong, S. Xia, Y. Yao, Solid State Ion. **307**, 73 (2017). https://doi.org/10.1016/j.ssi.2017.04.011
23. X. Xiong, Z. Wang, X. Yin, H. Guo, X. Li, Mater. Lett. **110**, 4 (2013). https://doi.org/10.1016/j.matlet.2013.07.098
24. L. Li, Y. Cao, H. Zheng, C. Feng, J. Mater. Sci.:Mater. Electron. **28**, 1925 (2017). https://doi.org/10.1007/s10854-016-5745-1
25. X. Lu, X. Li, Z. Wang, H. Guo, G. Yan, X. Yin, Appl. Surf. Sci. **297**, 182 (2014). https://doi.org/10.1016/j.apsusc.2014.01.121
26. G.-W. Yoo, B.-C. Jang, J.-T. Son, (2015) Ceram. Int. **41**:1913. https://doi.org/10.1016/j.ceramint.2014.09.077
27. J.J. Saavedra-Arias, N.K. Karan, D.K. Pradhan et al., J. Power Sources **183**, 761 (2008). https://doi.org/10.1016/j.jpowsour.2008.05.068
28. K.M. Shaju, G.V. Subba Rao, B.V.R. Chowdari, Electrochim. Acta **48**, 145 (2002). https://doi.org/10.1016/S0013-4686(02)00593-5
29. H. Liu, J. Li, Z. Zhang, Z. Gong, Y. Yang, Electrochim. Acta **49**, 1151 (2004). https://doi.org/10.1016/j.electacta.2003.11.001
30. L. Croguennec, E. Suard, P. Willmann, C. Delmas, Chem. Mater. **14**, 2149 (2002). https://doi.org/10.1021/cm011265v
31. Y. Yao, H. Liu, G. Li, H. Peng, K. Chen, Electrochim. Acta **113**, 340 (2013). https://doi.org/10.1016/j.electacta.2013.09.071
32. F. Wu, M. Wang, Y. Su, S. Chen, B. Xu, J. Power Sources **191**, 628 (2009). https://doi.org/10.1016/j.jpowsour.2009.02.063